

Available online at www.sciencedirect.com

ScienceDirect

www.elsevier.com/locate/jes

Facile synthesis of Ag-modified manganese oxide for effective catalytic ozone decomposition

Xiaotong Li^{1,2}, Jinzhu Ma^{2,3,4,*}, Changbin Zhang^{2,4}, Runduo Zhang¹, Hong He^{2,3,4}

1. State Key Laboratory of Chemical Resource Engineering, Beijing Key Laboratory of Energy Environmental Catalysis, Beijing University of Chemical Technology, Beijing 100029, China

2. State Key Joint Laboratory of Environment Simulation and Pollution Control, Research Center for Eco-Environmental Sciences, Chinese Academy of Sciences, Beijing 100085, China

3. Center for Excellence in Regional Atmospheric Environment, Institute of Urban Environment, Chinese Academy of Sciences, Xiamen 361021, China

4. University of Chinese Academy of Sciences, Beijing 100049, China

ARTICLE INFO

Article history:

Received 19 October 2018

Revised 14 December 2018

Accepted 17 December 2018

Available online 27 December 2018

Keywords:

Ag-modified manganese oxide

Ag-Hollandite

Ozone decomposition

Co-precipitation method

ABSTRACT

O₃ decomposition catalysts with excellent performance still need to be developed. In this study, Ag-modified manganese oxides (AgMnO_x) were synthesized by a simple co-precipitation method. The effect of calcination temperature on the activity of MnO_x and AgMnO_x catalysts was investigated. The effect of the amount of Ag addition on the activity and structure of the catalysts was further studied by activity testing and characterization by a variety of techniques. The activity of 8%AgMnO_x for ozone decomposition was significantly enhanced due to the formation of the Ag_{1.8}Mn₈O₁₆ structure, indicating that this phase has excellent performance for ozone decomposition. The weight content of Ag_{1.8}Mn₈O₁₆ in the 8%AgMnO_x catalyst was only about 33.76%, which further indicates the excellent performance of the Ag_{1.8}Mn₈O₁₆ phase for ozone decomposition. The H₂ temperature programmed reduction (H₂-TPR) results indicated that the reducibility of the catalysts increased due to the formation of the Ag_{1.8}Mn₈O₁₆ structure. This study provides guidance for a follow-up study on Ag-modified manganese oxide catalysts for ozone decomposition.

© 2018 The Research Center for Eco-Environmental Sciences, Chinese Academy of Sciences.

Published by Elsevier B.V.

Introduction

Ozone is a double-edged sword: ozone in the stratosphere can protect the creatures of the earth from ultraviolet radiation; however, ozone near the ground is a threat to human health. Studies have shown that long-term exposure to even low concentrations of ozone can have adverse effects on human health, such as increasing the incidence of respiratory diseases (Magzamen et al., 2017), affecting the cardiovascular system (Berman et al., 2012; Hoffmann et al., 2012), and harming

cardiopulmonary function (Fadeyi, 2015). Outdoor ozone pollution is mainly derived from photochemical reactions involving nitrogen oxides (NO_x) and volatile organic compounds (VOCs) (Cooper et al., 2010). Electrostatic equipment, ultraviolet disinfection devices and related ozone air purifiers make a great contribution to indoor ozone pollution (Fadeyi, 2015; Tuomi et al., 2000; Yu et al., 2011). The daily maximum 8-hr average surface O₃ concentration in the Chinese Ambient Air Quality Standards (GB3095-2012) Grade II standards and 1-hr average O₃ concentration in the Chinese Indoor Air Quality Standards (GB/T

* Corresponding author. E-mail: jzma@rcees.ac.cn. (Jinzhu Ma).

18883-2002) is ~82 ppbV. Therefore, the study of ozone removal is of great significance to human health and environmental protection.

According to long-term research, catalytic decomposition is considered to be a safe, efficient and economical approach among a variety of ozone removal methods. Catalysts for ozone decomposition principally include transition metal oxides (e.g. MnO_2 (Wang et al., 2015; Ma et al., 2017; Zhu et al., 2017; Li et al., 2018), Co_3O_4 (Tang et al., 2014), Cu_2O (Gong et al., 2017, 2018), Fe_2O_3 (Mehandjiev and Naidenov, 1992; Lian et al., 2015) and NiO (Mehandjiev et al., 2001)) and noble metals (e.g. Ag (Imamura et al., 1991; Naydenov et al., 2008), Au (Hao et al., 2001; Zhang et al., 2009) and Pd (Yu et al., 2009; Zhou et al., 2013)). Noble metal catalysts have excellent activity for ozone decomposition and good water resistance compared to other catalysts, but their exorbitant prices limit practical application (Naydenov et al., 2008; Hao et al., 2001; Chang and Lin, 2005). Imamura et al. (1991, 1988) found that the activity of Ag_2O catalysts for ozone decomposition is better than that of NiO , Co_3O_4 , Mn_2O_3 , Fe_2O_3 and other metal oxides, and gradually increases as the reaction proceeds, which is attributed to the oxygen species on the surface of Ag oxides being more weakly bound compared with other metal oxides, giving them greater mobility to react with O_3 to accelerate its decomposition. Besides, Ag has a lower price than other noble metals. Thus, Ag was selected in this study as the active component added to catalysts to increase activity.

Hollandite-type manganese oxides are a kind of octahedral molecular sieve composed of a one-dimensional tunnel structure constructed of double chains of edge-sharing MnO_6 octahedra, with the cations in the tunnels occupying the center of the cubic cage formed by MnO_6 octahedra and coordinated with eight oxygen anions (Li and King, 2005). Hollandite-type manganese oxides have been applied in DeNO_x processes and soot oxidation (Wang et al., 2011; Huang et al., 2013; Liu et al., 2018). $\text{Ag}_{1.8}\text{Mn}_8\text{O}_{16}$ is a kind of special hollandite structure in which Ag ions are located on the common faces of the cube and coordinate with four oxygen atoms (Chang and Jansen, 1984). Li and King (2005) synthesized the $\text{Ag}_{1.8}\text{Mn}_8\text{O}_{16}$ material by ion exchange of cryptomelane in AgNO_3 melt, and found that it has excellent performance for low-temperature SO_2 absorption and the oxidation of CO and NO. Chen et al. (2007) prepared Ag-hollandite nanofibers through a simple hydrothermal reaction between $\text{Mn}(\text{NO}_3)_2$ and AgMnO_4 and found that the material has excellent catalytic performance in ethanol oxidation. Sun et al. (2011) also synthesized $\text{Ag}_{1.8}\text{Mn}_8\text{O}_{16}$ nanorods by a facile hydrothermal route, and discovered that the products had electrochemical lithium-storage capabilities. Huang et al. (2012) successfully fabricated active single-atom Ag chains in the openings of the Ag-modified hollandite-type manganese oxide (Ag-HMO) tunnels by simple thermal processing of Ag particles, and found that the single-atom Ag catalyst had excellent activity for HCHO oxidation at low temperatures, which was ascribed to the high activation ability toward both lattice oxygen and molecule oxygen. However, the performance of the $\text{Ag}_{1.8}\text{Mn}_8\text{O}_{16}$ material in ozone decomposition has not been studied.

In this work, catalysts containing $\text{Ag}_{1.8}\text{Mn}_8\text{O}_{16}$ and $\alpha\text{-Mn}_2\text{O}_3$ were successfully synthesized by a simple co-precipitation method, and results showed that the activity of the catalysts for ozone decomposition was markedly enhanced due to the formation of $\text{Ag}_{1.8}\text{Mn}_8\text{O}_{16}$. The above results indicate that the $\text{Ag}_{1.8}\text{Mn}_8\text{O}_{16}$ phase has excellent performance for ozone decomposition, which can guide the follow-up study of Ag-modified manganese oxides.

1. Materials and methods

1.1. Preparation of catalysts

The AgMnO_x catalysts were prepared by a co-precipitation method, and $\text{MnSO}_4 \cdot \text{H}_2\text{O}$, AgNO_3 and Na_2CO_3 were selected as raw materials. The specific synthesis process of AgMnO_x catalysts is as follows: 10.5 g of $\text{MnSO}_4 \cdot \text{H}_2\text{O}$ was dissolved in 250 mL deionized water under stirring, then 85.87 mg (1%Ag), 173.49 mg (2%Ag), 354.20 mg (4%Ag), 542.61 mg (6%Ag) or 739.21 mg AgNO_3 (8%Ag) was added, followed by stirring magnetically for about 30 min until the solution became homogeneous, and the obtained solution was named as A; 9.3 g of Na_2CO_3 was dissolved in 150 mL deionized water under stirring to obtain a homogeneous solution of B; then solution B was added to solution A drop by drop at a constant dropping rate, and a mixed precipitate of MnCO_3 and Ag_2CO_3 was obtained as the reaction progressed. The final pH value of the supernatant liquor was about 8. Next the resulting precipitates were filtered, washed, dried at 80°C for 12 hr and calcined at 600°C for 3 hr. The above prepared catalysts were named 1% AgMnO_x , 2% AgMnO_x , 4% AgMnO_x , 6% AgMnO_x and 8% AgMnO_x , respectively. The MnO_x catalyst was prepared by a similar synthetic procedure as AgMnO_x without adding AgNO_3 during the preparation of solution A. Furthermore, the MnO_x and 8% AgMnO_x catalyst precursors were also calcined at 300, 400, 500 and 900°C for 3 hr to investigate the effect of different calcination temperatures.

1.2. Catalyst characterization

The thermostability of precipitates was tested by a thermal gravimetric analyzer/dynamic stability control STAR[®] system (TGA/DSC 1 STAR[®] system, METTLER TOLEDO, Switzerland) at $10^\circ\text{C}/\text{min}$ heating rate from 30 to 1000°C under 50 mL/min of flowing air. The obtained precipitates containing MnCO_3 and Ag_2CO_3 were used as the test sample.

The crystalline structure of catalysts was determined by X-ray powder diffraction (XRD) (D8-Advance, Bruker, Germany) using $\text{Cu K}\alpha$ ($\lambda = 0.15406$ nm) radiation at a tube voltage of 40 kV and current of 40 mA in the 2θ range $10\text{--}80^\circ$ with a step size of 0.02° .

The Raman spectra of catalysts were recorded on a homemade ultraviolet resonance Raman spectrometer (UVRDLPC-DL-03) and a charge coupled device (CCD) detector cooled to 60°C by liquid nitrogen. The Stokes Raman signal of Teflon at 1378 cm^{-1} was used to calibrate the instrument. The exciting radiation was a continuous diode-pumped solid state (DPSS) laser beam (532 nm) with about 40 mW power. The

spectrum was recorded for 10 min with the resolution of 2.0 cm^{-1} .

A Quantachrome physisorption analyzer (Autosorb-iQ-1MP, Quantachrome, USA) was used to obtain the specific surface area and pore structure of the catalysts. The catalysts were degassed at 280°C for 6 hr before measurement. The surface area (S_{BET}) was obtained by the Brunauer–Emmett–Teller (BET) equation from data in the 0.05–0.35 partial pressure range.

A field emission scanning electron microscope (FESEM) (SU8020, HITACHI, Japan) with the accelerating voltage of 3 kV was used to observe the morphologies of the catalysts.

The temperature programmed H_2 reduction (H_2 -TPR) experiments were conducted using a chemisorption analyzer (AutoChem II, Micromeritics, USA) equipped with a Thermal Conductivity Detector (TCD). About 50 mg of 40–60 mesh catalyst was used to conduct the experiments. Firstly, the surface-adsorbed water was removed by heating in air at 300°C for 1 hr. Then the sample was cooled down to 50°C , and the temperature programmed reduction process were conducted in 5 vol.% H_2 in Ar with a flow rate of 50 mL/min.

The temperature programmed desorption of O_2 experiment (O_2 -TPD) was carried out to observe the desorption of oxygen, and the signal for O_2 was detected with a mass spectrometer (Cirrus, MKS, USA). Firstly, about 150 mg of catalyst was pretreated with helium at 105°C for 30 min. Next the catalyst was cooled down to 50°C , and then was allowed to adsorb oxygen in a mixture of O_2/He of 50 mL/min for 1 hr. After the sample was purged with helium for 30 min, desorption of O_2 from the catalyst was monitored as the temperature was ramped from 50 to 850°C in helium at a heating rate of $10^\circ\text{C}/\text{min}$.

The imaging X-ray photoelectron spectrometer (XPS) (Axis Ultra, Kratos Analytical Ltd., UK) was used to determine the state and the surface content of atom.

The actual addition of Ag of AgMnO_x catalysts was detected using an inductively coupled plasma spectrometer (ICP) (720, Varian, USA). All samples were dissolved using concentrated nitric acid before being tested.

1.3. Catalyst activity for ozone decomposition

All the activity tests were conducted in a fixed-bed continuous flow quartz reactor (4 mm inner diameter) using 100 mg of catalyst with size of 40–60 mesh at room temperature (30°C) under a gas flow of 1400 mL/min and relative humidity of 65%. The space velocity was calculated to be $840,000 \text{ hr}^{-1}$. The relative humidity of the gas stream was maintained at 65% by controlling the flow of wet gas, which was measured with a humidity probe (HMP110, Vaisala OYJ, Finland). The ozone was generated by low-pressure ultraviolet lamps, and the concentration was maintained at $40 \pm 2 \text{ ppmV}$. An ozone monitor (Model 202, 2B Technologies, USA) was used to monitor the inlet and outlet ozone concentrations. The ozone conversion (CONV_{O_3}) was calculated by the following equation:

$$\text{CONV}_{\text{O}_3} = \frac{C_{\text{in}} - C_{\text{out}}}{C_{\text{in}}} \times 100\% \quad (1)$$

where, C_{in} (ppbV) and C_{out} (ppbV) are inlet and outlet concentrations of ozone, respectively.

2. Results and discussion

2.1. Effect of calcination temperature

Fig. 1 shows the thermogravimetry/DSC (TG/DSC) profiles of the MnO_x catalyst precursor (MnCO_3), which were measured to investigate its thermal stability. The weight loss can be categorized into four segments. The weight loss below 300°C can be attributed to the removal of physically adsorbed water and desorption of chemically bonded water (Jia et al., 2016). When the temperature rises to 400°C , the corresponding weight loss can be ascribed to the evolution of lattice oxygen and phase transformation from MnCO_3 to MnO_2 (Figs. 2b and 3b). When the temperature further increases to 600°C , the corresponding weight loss is due to the evolution of lattice oxygen and phase transformation from MnO_2 to Mn_2O_3 (Figs. 2b and 3b). When the temperature is higher than 900°C , the corresponding weight loss can be due to the evolution of lattice oxygen and phase transformation from Mn_2O_3 to MnO .

According to the TG/DSC results, MnO_x tended to lose carbon dioxide and oxygen ($\text{MnCO}_3 \rightarrow \text{MnO}_2 \rightarrow \text{Mn}_2\text{O}_3 \rightarrow \text{Mn}_3\text{O}_4$) when calcined at elevated temperature. As is shown in Fig. 2a, the activity of the MnO_x catalyst for ozone decomposition gradually decreased as the calcination temperature increased. When the calcination temperature was 300°C , the catalyst was still MnCO_3 (JCPDS 44-1472) and its conversion level for 40 ppmV ozone was about 67% under a space velocity of $840,000 \text{ hr}^{-1}$ and relative humidity (RH) of 65% after 6 hr at room temperature. When the calcination temperature increased to 400°C , the catalyst consisted of MnCO_3 and MnO_2 (JCPDS 30-0820), indicating that MnCO_3 gradually transforms into MnO_2 at this temperature, and its activity was about 70%. When the calcination temperature further increased to 500°C , the catalyst consisted of MnO_2 and Mn_5O_8 (JCPDS 39-1218), indicating that MnO_2 partly transforms into Mn_5O_8 at this temperature, and its activity for ozone decomposition decreased to 31%. When the calcination

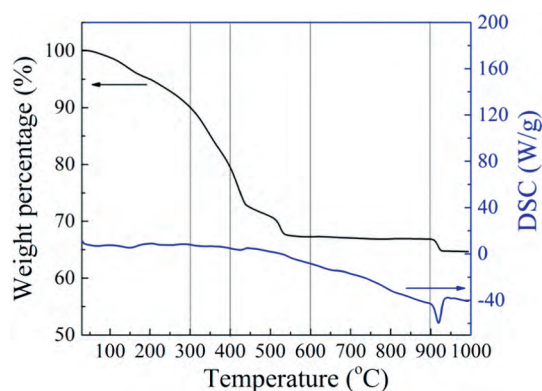


Fig. 1 – Thermogravimetry/Dynamic stability control (TG/DSC) curves of the MnO_x catalyst.

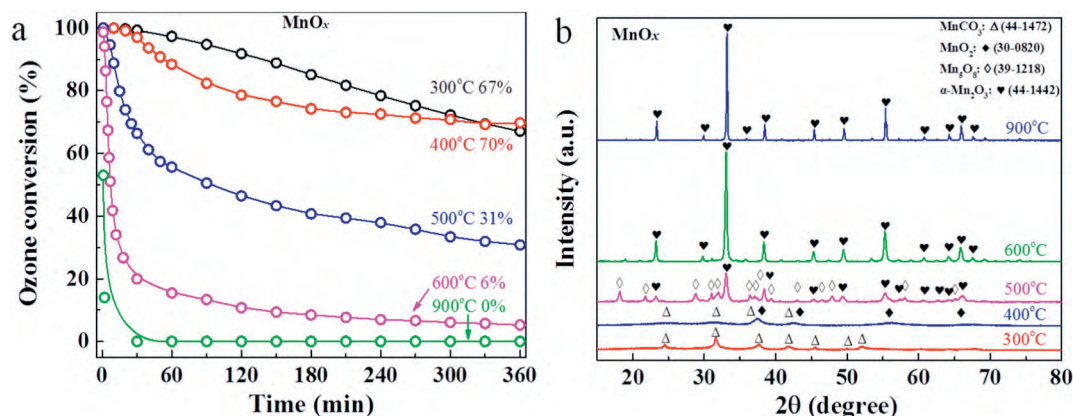


Fig. 2 – (a) Effect of calcination temperature on the activity of MnO_x catalyst. Conditions: ozone inlet concentration 40 ppmV, temperature 30°C, relative humidity 65%, space velocity 840,000 hr⁻¹; **(b)** X-ray powder diffraction (XRD) patterns of MnO_x catalyst calcined at different temperature.

temperature further increased to 600 and 900°C, the MnO_x totally transformed into α-Mn₂O₃ (JCPDS 44-1442), and the conversion level for ozone decreased to 6% and 0%, respectively.

The effect of calcination temperature on the conversion of ozone and crystal structure of the 8%AgMnO_x catalyst is shown in Fig. 3. When the calcination temperature was 300 and 400°C, the 8%AgMnO_x catalyst mainly consisted of MnCO₃ and a mixture of MnCO₃ and MnO₂, respectively, and the diffraction peaks representing related species of Ag were not observed, which revealed that the content was below the detection limits of the XRD instrument, or that Ag-containing species were finely dispersed over the MnO_x. The ozone conversion of the above catalyst calcined at 300 and 400°C was 71% and 78%, respectively, which indicates that adding Ag at these two temperatures does not increase the activity to a great extent. When the 8%AgMnO_x catalyst precursor was calcined at 500°C, the catalyst consisted of α-Mn₂O₃, Mn₃O₄ and Ag_{1.8}Mn₈O₁₆ (JCPDS 77-1987), and the ozone decomposition activity was only 39%, indicating that the addition of Ag

at this temperature also does not increase the activity much. When the calcination temperature increased to 600°C, the 8% AgMnO_x catalyst, composed of α-Mn₂O₃ and Ag_{1.8}Mn₈O₁₆, was found to have the best activity for ozone decomposition among all catalysts. The pure MnO_x catalyst calcined at 600°C was totally converted into α-Mn₂O₃, which indicates that the addition of Ag can restrain the conversion of MnO₂ to Mn₂O₃. Furthermore, the addition of Ag increased the activity from 6% to 81% at the calcination temperature of 600°C. When the calcination temperature further rose to 900°C, the 8%AgMnO_x catalyst was mainly composed of α-Mn₂O₃ and Mn₃O₄ (JCPDS 24-0734), and the related species of Ag could not be observed. The content of Ag may be below the detection limit of the XRD instrument, or the corresponding species could be finely dispersed over the catalyst. The addition of Ag increases the activity from 0% to 39% at the calcining temperature of 900°C. According to the above results, the 8%AgMnO_x catalyst calcined at 600°C had the best activity for ozone decomposition among all the catalysts and the maximum improvement

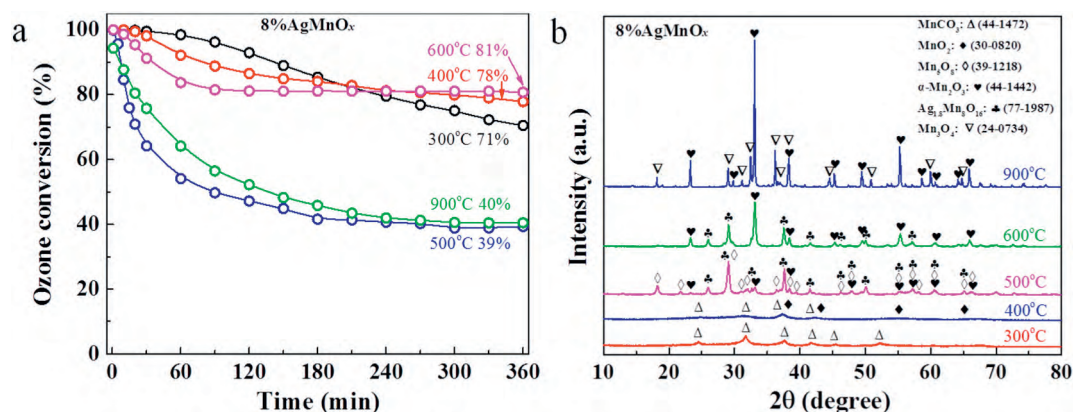


Fig. 3 – (a) Effect of calcination temperature on the activity of the 8%AgMnO_x catalyst. Conditions: ozone inlet concentration 40 ppmV, temperature 30°C, relative humidity 65%, space velocity 840,000 hr⁻¹; **(b)** XRD patterns of 8%AgMnO_x catalyst calcined at different temperatures.

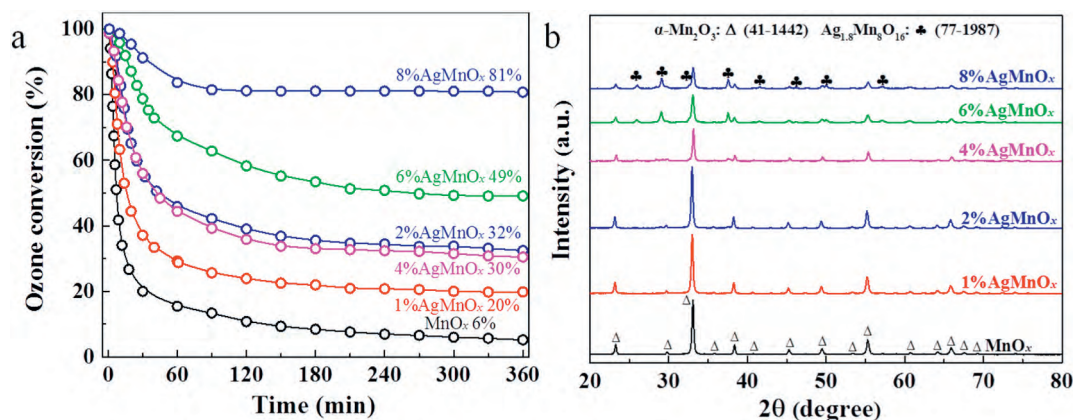


Fig. 4 – (a) Conversion of ozone on the MnO_x, 1%AgMnO_x, 2%AgMnO_x, 4%AgMnO_x, 6%AgMnO_x and 8%AgMnO_x catalysts. Conditions: ozone inlet concentration 40 ppmV, temperature 30°C, relative humidity 65%, space velocity 840,000 hr⁻¹; (b) XRD patterns of the MnO_x, 1%AgMnO_x, 2%AgMnO_x, 4%AgMnO_x, 6%AgMnO_x and 8%AgMnO_x catalysts.

in activity compared to the MnO_x catalyst. Therefore, the calcination temperature of 600°C was concluded to be optimal and was used during subsequent preparation.

2.2. Effect of the amount of Ag addition

The activity of AgMnO_x with different contents of Ag for ozone decomposition is shown in Fig. 4a. It is evident that the activity gradually improved as the content of Ag increased. The catalysts with Ag addition of 0%, 1%, 2%, 4%, 6% and 8% showed 6%, 20%, 32%, 30%, 49% and 81% conversion for 40 ppmV ozone under a space velocity of 840,000 hr⁻¹ after 6 hr at room temperature and RH = 65%, respectively. As is shown in Fig. 4b, the MnO_x catalyst is comprised of α-Mn₂O₃. The diffraction peaks of α-Mn₂O₃ were also observed in the 1% AgMnO_x and 2%AgMnO_x catalysts, but the diffraction peaks of Ag species were not observed, which revealed that the content of Ag species was below the detection limits of the XRD instrument, or that they were finely dispersed over the MnO_x surface. The diffraction peaks of Ag_{1.8}Mn₈O₁₆ began to appear in the 4%AgMnO_x catalyst, indicating that Ag_{1.8}Mn₈O₁₆ began to form. When the content of Ag increased to 6% or 8%, the diffraction peaks of Ag_{1.8}Mn₈O₁₆ become narrower and stronger, indicating that Ag_{1.8}Mn₈O₁₆ was well-formed. When the Ag_{1.8}Mn₈O₁₆ was well-formed, the activity of the catalyst markedly increased. Therefore, the Ag_{1.8}Mn₈O₁₆ phase is the key component to improve the activity of the catalyst. Furthermore, when the amount of Ag addition was 4%, 6% and 8%, the diffraction peaks of α-Mn₂O₃ became weakened, indicating that the crystallinity decreased, which is also beneficial to the activity.

Raman spectra of the MnO_x and 8%AgMnO_x catalysts were obtained to further observe the structure of the catalysts and are shown in Fig. 5. Bands at 178 and 306 cm⁻¹ can be attributed to the out-of-plane bending modes, and bands appearing at 635 and 693 cm⁻¹ can be ascribed to the symmetric stretching modes of Mn₂O₃ (Buciuman et al., 1999; Kapteijn et al., 1994; Li et al., 2017; Kolathodi et al., 2016). The above results are similar to those in previous literature (Kapteijn et al., 1994), and indicate that the obtained MnO_x catalyst is Mn₂O₃ without

formation of other MnO_x phases. Bands at 206 and 587 cm⁻¹ appeared in the Raman spectra of the 8%AgMnO_x catalyst, and the two bands were ascribed to the deformation vibration of the metal-oxygen chain of Mn–O–Mn and the stretching vibration of the MnO₆ octahedron, respectively (Zhu et al., 2017; Xie et al., 2015). According to previous literature, Ag_{1.8}Mn₈O₁₆ shows a zeolite-like structure that is comprised of a Mn₈O₁₆ skeletal framework of corner- and edge-sharing MnO₆ octahedra, and Ag ions in the channels participate in the coordination (Chang and Jansen, 1984; Qu et al., 2013). The new bands further demonstrate the formation of Ag_{1.8}Mn₈O₁₆. The Raman results are consistent with the XRD results.

2.3. Specific surface area and morphology

The N₂ adsorption–desorption isotherms of the MnO_x, 1% AgMnO_x, 2%AgMnO_x, 4%AgMnO_x, 6%AgMnO_x and 8%AgMnO_x catalysts are shown in Appendix A Fig. S1. All the catalysts have similar N₂ adsorption/desorption isotherms, showing the characteristics of a type II isotherm with a H3 hysteresis loop. The above phenomenon is related to the formation of slit-

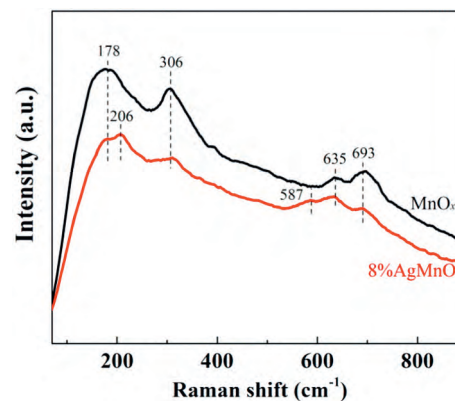


Fig. 5 – Raman spectra of the MnO_x and 8%AgMnO_x catalysts.

Table 1 – Brunauer–Emmett–Teller (BET) surface area and temperature programmed H₂ reduction (H₂-TPR) results of the MnO_x, 1%AgMnO_x, 2%AgMnO_x, 4%AgMnO_x, 6%AgMnO_x and 8%AgMnO_x catalysts.

Catalyst	BET	H ₂ -TPR
	Surface area (m ² /g)	Total H ₂ consumption (mmol/g)
MnO _x	21	5.43
1%AgMnO _x	27	5.4
2%AgMnO _x	27	5.5
4%AgMnO _x	25	5.82
6%AgMnO _x	31	6.32
8%AgMnO _x	32	6.52

shaped pores in the materials, which can cause the appearance of macropores (Xie et al., 2017). The specific surface areas are shown in Table 1. The specific surface areas of catalysts slightly increased with the addition of Ag, which can be related to the formation of Ag_{1.8}Mn₈O₁₆.

As is shown in Fig. 6, the morphology of catalysts was observed by FESEM. The MnO_x catalyst consisted of aggregated nanoparticles. When the content of Ag was 1% or 2%, the morphology of 1%AgMnO_x and 2%AgMnO_x catalysts was still aggregated nanoparticles. When the content of Ag continued to increase to 4%, short, thick nanorods begin to appear in the 4%AgMnO_x catalyst. The short thick nanorods increased in number in 6%AgMnO_x, and the 8%AgMnO_x catalyst had the most nanorods. According to previous literature, Ag_{1.8}Mn₈O₁₆ has a nanorod morphology (Li and King, 2005). Therefore, the nanorods appearing in the 4%

AgMnO_x, 6%AgMnO_x and 8%AgMnO_x catalysts can be attributed to formation of the Ag_{1.8}Mn₈O₁₆ structure.

2.4. Temperature programmed studies

As is shown in Fig. 7, temperature programmed reduction was conducted to investigate the reducibility of catalysts. The MnO_x catalyst has two reduction peaks at 316 and 418°C, and the H₂ consumption of peak I and peak II is 1.85 and 3.58 mmol/g, respectively. The H₂ consumption of peak II is about twice that of peak I, so the reduction path of the MnO_x catalyst is Mn₂O₃ to Mn₃O₄, and then Mn₃O₄ to MnO. When Ag was added in the MnO_x catalyst, three reduction peaks could be observed, and the temperature of every reduction peak obviously decreased. The new reduction peak I of 1%AgMnO_x and 2%AgMnO_x catalysts at 170 and 163°C can be attributed to the reduction of Ag⁺ to Ag⁰ (Qu et al., 2013). The new reduction peak III of 1%AgMnO_x and 2%AgMnO_x catalysts at 313 and 297°C became smaller compared with the MnO_x catalyst, and the new reduction peak II of these two catalysts gradually became larger, which can be ascribed to the addition of Ag facilitating the direct reduction of a fraction of Mn₂O₃ to MnO (Qu et al., 2013). According to the XRD and Raman results, the Ag_{1.8}Mn₈O₁₆ structure formed in the 6%AgMnO_x and 8%AgMnO_x catalysts. The reduction of the Ag_{1.8}Mn₈O₁₆ phase occurs in two steps: firstly, Ag⁺ is reduced to Ag⁰, and Mn⁴⁺ is reduced to Mn³⁺, then, Mn³⁺ is reduced to Mn²⁺ (Huang et al., 2012). Thus, the reduction peak I of 6%AgMnO_x and 8%AgMnO_x catalysts at 166°C can be attributed to the reduction of Ag⁺ to Ag⁰ and Mn⁴⁺ to Mn³⁺ in Ag_{1.8}Mn₈O₁₆, and the reduction peak II of 6%AgMnO_x and 8%AgMnO_x catalysts at 185 and 187°C can be ascribed to the reduction of Mn³⁺ to Mn²⁺ in Ag_{1.8}Mn₈O₁₆ and Mn₂O₃ to Mn₃O₄ in α-Mn₂O₃. The reduction

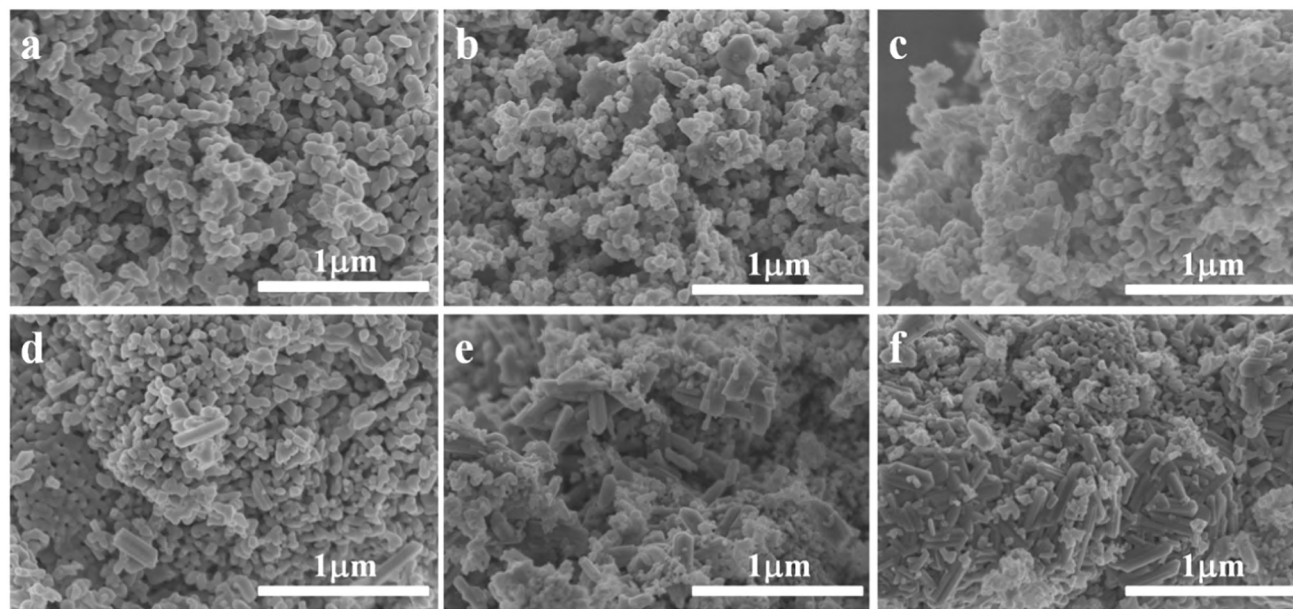


Fig. 6 – Scanning electron microscope (SEM) images of (a) MnO_x, (b) 1%AgMnO_x, (c) 2%AgMnO_x, (d) 4%AgMnO_x, (e) 6%AgMnO_x and (f) 8%AgMnO_x.

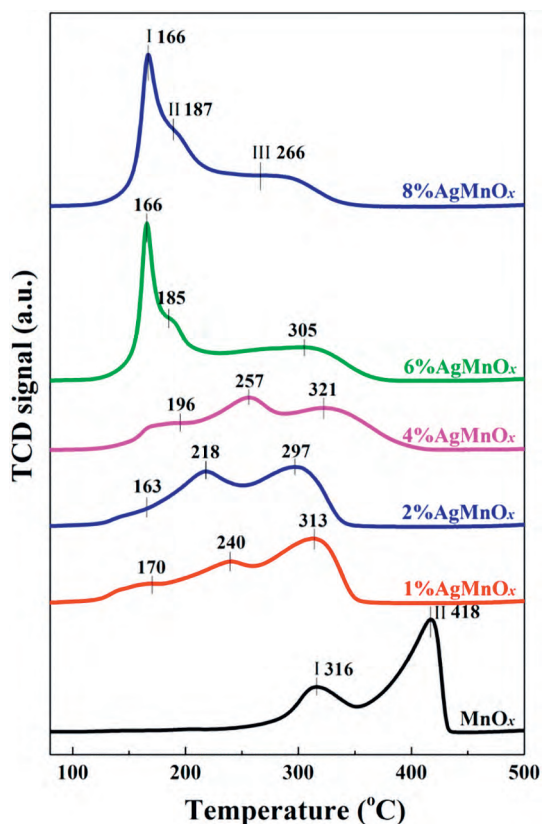


Fig. 7 – H₂-TPR profiles of the MnO_x, 1%AgMnO_x, 2%AgMnO_x, 4%AgMnO_x, 6%AgMnO_x and 8%AgMnO_x catalysts.

peak III of 6%AgMnO_x and 8%AgMnO_x catalysts at 305 and 266°C is attributed to the reduction of Mn₃O₄ to MnO. The Ag_{1.8}Mn₈O₁₆ structure began to form in 4%AgMnO_x, so the reduction peak I of 4%AgMnO_x catalyst at 196°C can be attributed to the reduction of the Ag_{1.8}Mn₈O₁₆ phase. Meanwhile, a portion of the Ag atoms did not form the Ag_{1.8}Mn₈O₁₆ structure, and this Ag can promote the direct reduction of a fraction of Mn₂O₃ to MnO, which makes the reduction peak II bigger and causes reduction peak III to become smaller. The decline of the reduction temperature for every peak can be attributed to the Ag species facilitating the reduction of manganese oxides and the mobility of lattice oxygen species. Activation of hydrogen on the surface of Ag species depends on the hydrogen spillover to migrate to the surface of the manganese oxides and participate in the reduction process (Li et al., 2016; Bai et al., 2016). Furthermore, the new reduction peak I for AgMnO_x catalysts gradually becomes stronger as the content of Ag increases. Meanwhile, the total H₂ consumption also increases as the content of Ag increases (Table 1). The above phenomena further demonstrate the increase in the amount of Ag_{1.8}Mn₈O₁₆. The Ag_{1.8}Mn₈O₁₆ component is recognized as the active ingredient. The 8%AgMnO_x catalyst has the most Ag_{1.8}Mn₈O₁₆, so the 8%AgMnO_x catalyst has the best activity. The above results are consistent with the XRD, Raman and BET results.

The temperature programmed desorption results of O₂ of the MnO_x, 1%AgMnO_x, 2%AgMnO_x, 4%AgMnO_x, 6%AgMnO_x

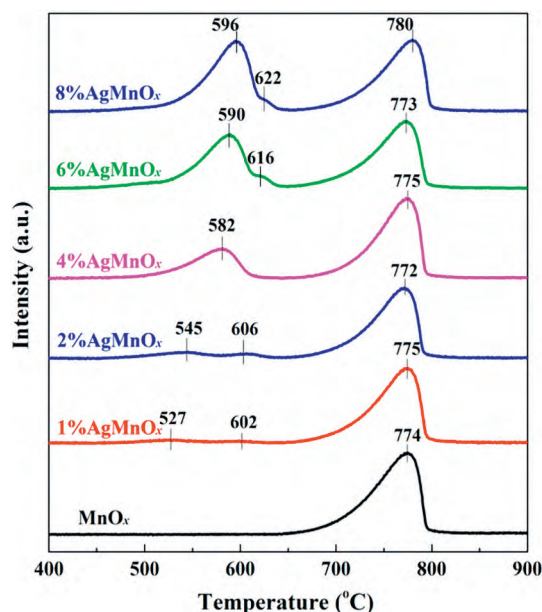


Fig. 8 – Temperature programmed desorption of O₂ (O₂-TPD) profiles of the MnO_x, 1%AgMnO_x, 2%AgMnO_x, 4%AgMnO_x, 6%AgMnO_x and 8%AgMnO_x catalysts.

and 8%AgMnO_x catalysts are shown in Fig. 8. The MnO_x catalyst has only one desorption peak at 774°C, which is attributed to the transformation of Mn₂O₃ to MnO. When Ag was added into the MnO_x catalyst, the desorption peaks between 520 and 630°C began to appear. The first two desorption peaks are ascribed to the conversion of Ag_{1.8}Mn₈O₁₆ to Mn₂O₃ and Ag⁰. The last desorption peak for AgMnO_x is still due to the transformation of Mn₂O₃ to MnO. Meanwhile, the first two desorption peaks gradually shift to higher temperature and become larger, which is related to the formation of Ag_{1.8}Mn₈O₁₆. The structure of Ag_{1.8}Mn₈O₁₆ becomes more stable as the content of Ag increases. No obvious shift is observed in the last desorption peak. The above results further demonstrate the formation of Ag_{1.8}Mn₈O₁₆, which is consistent with the XRD, Raman, BET and H₂-TPR results.

2.5. Surface atom oxidation state

As is shown in Fig. 9, the XPS spectra were used to determine the surface atom oxidation state of the catalysts. The Mn 3s spectra of catalysts were analyzed to estimate the average oxidation state (AOS) of Mn according to the following formula:

$$\text{AOS} = 8.956 - 1.126\Delta E_s \quad (2)$$

where, ΔE_s is the binding energy difference between the doublet Mn 3s peaks (Jia et al., 2016). The AOS of the MnO_x, 1%AgMnO_x, 2%AgMnO_x, 4%AgMnO_x, 6%AgMnO_x and 8%AgMnO_x catalysts is 2.80, 2.81, 2.82, 2.83, 3.02 and 3.03, respectively. The AOS of the MnO_x, 1%AgMnO_x, 2%AgMnO_x, 4%AgMnO_x catalysts slightly increased with the increase in Ag addition, but the AOS increased to 3.02 and 3.03 from 2.80

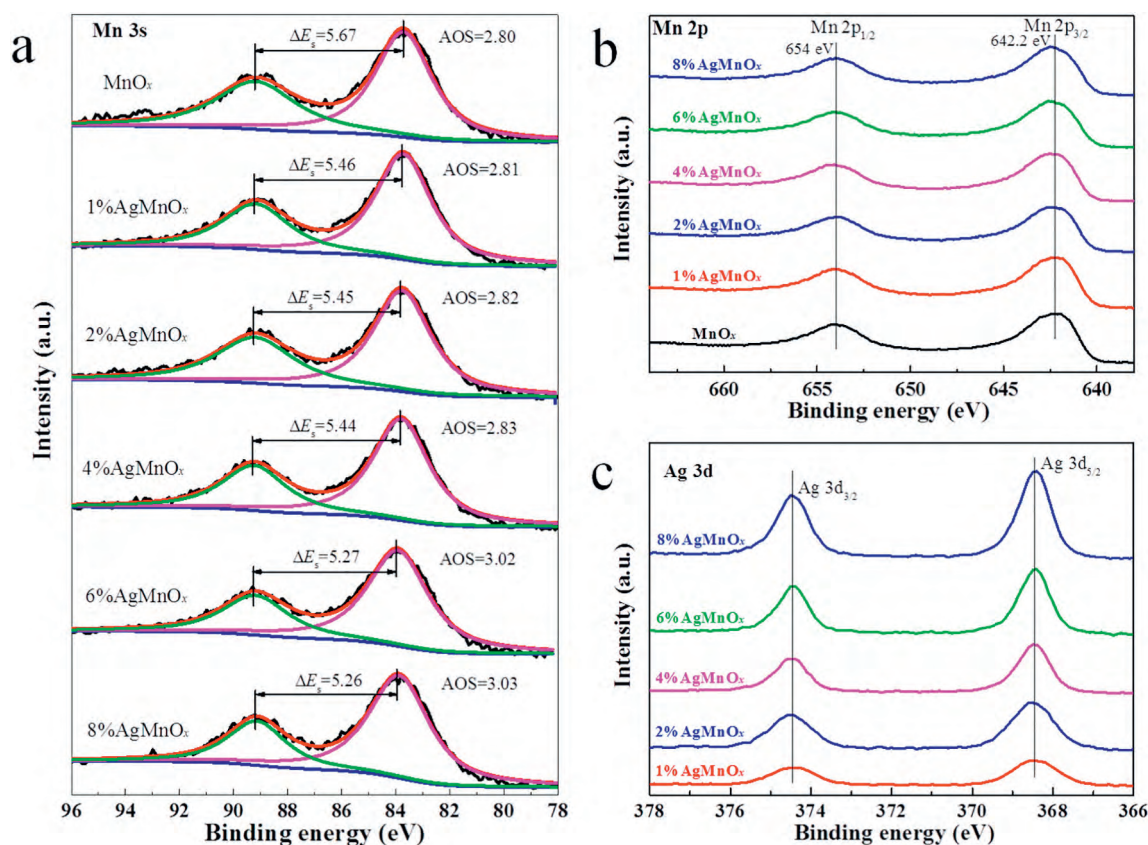


Fig. 9 – (a) Mn 3s (b) Mn 2p (c) Ag 3d X-ray photoelectron spectrometer (XPS) spectra of the MnO_x , 1% AgMnO_x , 2% AgMnO_x , 4% AgMnO_x , 6% AgMnO_x and 8% AgMnO_x catalysts. AOS: average oxidation state; ΔE_s : binding energy difference between the doublet Mn 3s peaks.

when the content of Ag increased to 6% and 8%. The above results also indicate that $\text{Ag}_{1.8}\text{Mn}_8\text{O}_{16}$ was well-formed in the 6% AgMnO_x and 8% AgMnO_x catalysts. Fig. 9b shows that the two different peaks corresponding to Mn $2p_{1/2}$ and Mn $2p_{3/2}$ are located at 654 and 642.2 eV, which is attributed to spin-orbit splitting. The spin-orbit splitting value is 11.8 eV, which is almost the same band gap energy as manganese (III) oxides (Li et al., 2017; Kolathodi et al., 2016). Fig. 9c shows that the binding energy of Ag $3d_{5/2}$ for AgMnO_x catalysts is 368.5 eV. The Ag $3d_{5/2}$ peak centers at 369 eV for Ag^0 and 368.5 eV for Ag^+ (Li et al., 2016). The above results indicate that the silver species are Ag^+ , which is consistent with the XRD and H_2 -TPR results.

Table 2 shows the mass percentage content of Ag on the surface of catalysts and in the bulk phase of catalysts, respectively. The ICP results represent the actual doping amounts of Ag in the catalysts, and the XPS results show the content of Ag on the surface of catalysts. The amount of Ag on the surface of 1% AgMnO_x and 2% AgMnO_x catalysts is far higher than the actual doping amount of Ag in the catalysts, which indicates that the Ag species of 1% AgMnO_x and 2% AgMnO_x catalysts mainly aggregate on the surface. When 4% Ag is added into the catalyst, the difference in the content of Ag on the surface and in the bulk goes down, so the aggregation of Ag species on the surface of catalyst is slightly alleviated, which is due to the gradual formation of

$\text{Ag}_{1.8}\text{Mn}_8\text{O}_{16}$. The amount of Ag on the surface and in the bulk for the 6% AgMnO_x and 8% AgMnO_x catalysts is almost identical. Therefore, the Ag species in the 6% AgMnO_x and 8% AgMnO_x catalysts do not aggregate on the surface of the catalysts and are homogeneously doped in the catalysts, which is due to the formation of $\text{Ag}_{1.8}\text{Mn}_8\text{O}_{16}$ causing Ag^+ to enter into its framework structure. The above results are consistent with the XRD and Raman results. Furthermore, the actual amounts of Ag in 4% AgMnO_x , 6% AgMnO_x and 8% AgMnO_x catalysts are 3.67, 5.52 and 7.37 wt.%, and the mass percentage of Ag in $\text{Ag}_{1.8}\text{Mn}_8\text{O}_{16}$ is 21.83%. If the doped Ag all goes into formation of $\text{Ag}_{1.8}\text{Mn}_8\text{O}_{16}$, the mass percentage of $\text{Ag}_{1.8}\text{Mn}_8\text{O}_{16}$ in the 4% AgMnO_x , 6% AgMnO_x and 8% AgMnO_x

Table 2 – Inductively coupled plasma spectrometer (ICP) and XPS results of the MnO_x , 1% AgMnO_x , 2% AgMnO_x , 4% AgMnO_x , 6% AgMnO_x and 8% AgMnO_x catalysts.

Catalyst	ICP	XPS
	Percentage (wt.%)	Percentage (wt.%)
1% AgMnO_x	0.99	2.74
2% AgMnO_x	1.83	5.53
4% AgMnO_x	3.67	4.06
6% AgMnO_x	5.52	5.20
8% AgMnO_x	7.37	7.00

catalysts rises to 16.81%, 25.29% and 33.76%, which further indicates that the $\text{Ag}_{1.8}\text{Mn}_8\text{O}_{16}$ phase is a highly effective active ingredient. Meanwhile, the catalytic performance of 4% AgMnO_x (30%), 6% AgMnO_x (49%) and 8% AgMnO_x (81%) catalysts gradually increases with the formation of $\text{Ag}_{1.8}\text{Mn}_8\text{O}_{16}$. Therefore, the synthesis and performance of pure $\text{Ag}_{1.8}\text{Mn}_8\text{O}_{16}$ will be investigated in future work.

3. Conclusions

Ag-modified manganese oxides (AgMnO_x) were synthesized by a simple co-precipitation method. The calcination temperature of 600°C was demonstrated to be the most appropriate for AgMnO_x . The activity of the 8% AgMnO_x catalyst was the best among all the catalysts, and the XRD and Raman results indicate that $\text{Ag}_{1.8}\text{Mn}_8\text{O}_{16}$ develops well when the addition of Ag reaches 8%. The activity and characteristic results indicate that $\text{Ag}_{1.8}\text{Mn}_8\text{O}_{16}$ is the key component enhancing the activity of catalysts. Meanwhile, the reducibility of the catalysts evidently increases on account of the formation of the $\text{Ag}_{1.8}\text{Mn}_8\text{O}_{16}$ structure. The weight content of $\text{Ag}_{1.8}\text{Mn}_8\text{O}_{16}$ in the 8% AgMnO_x catalyst is only 33.76% according to calculations based on ICP results, which further indicates the excellent performance of $\text{Ag}_{1.8}\text{Mn}_8\text{O}_{16}$ phase for ozone decomposition. The study has important guiding significance for subsequent research on Ag-modified manganese oxides.

Acknowledgments

This work was supported by the National Key R&D Program of China (Nos. 2016YFC0207104 and 2017YFC0211802), the National Natural Science Foundation of China (NSFC) (No. 21876191) and the Youth Innovation Promotion Association, Chinese Academy of Sciences (No. 2017064).

Appendix A. Supplementary data

Supplementary data to this article can be found online at <https://doi.org/10.1016/j.jes.2018.12.008>.

REFERENCES

Bai, B.Y., Qiao, Q., Arandiyani, H., Li, J.H., Hao, J.M., 2016. Three-dimensional ordered mesoporous MnO_2 -supported Ag nanoparticles for catalytic removal of formaldehyde. *Environ. Sci. Technol.* 50 (5), 2635–2640.

Berman, J.D., Fann, N., Hollingsworth, J.W., Pinkerton, K.E., Rom, W.N., Szema, A.M., et al., 2012. Health benefits from large-scale ozone reduction in the United States. *Environ. Health Perspect.* 120 (10), 1404–1410.

Buciuman, F., Patcas, F., Craciun, R., Zahn, D.R.T., 1999. Vibrational spectroscopy of bulk and supported manganese oxides. *Phys. Chem. Chem. Phys.* 1 (1), 185–190.

Chang, F.M., Jansen, M., 1984. $\text{Ag}_{1.8}\text{Mn}_8\text{O}_{16}$: square-planar coordinated Ag^+ ions in the channels of a novel hollandite variant. *Angew. Chem. Int. Ed.* 23 (11), 906–907.

Chang, C.L., Lin, T.S., 2005. Pt/Rh and Pd/Rh catalysts used for ozone decomposition and simultaneous elimination of ozone and carbon monoxide. *React. Kinet. Catal. Lett.* 86 (1), 91–98.

Chen, J.L., Tang, X.F., Liu, J.L., Zhan, E.S., Li, J., Huang, X.M., et al., 2007. Synthesis and characterization of Ag-hollandite nanofibers and its catalytic application in ethanol oxidation. *Chem. Mater.* 19 (17), 4292–4299.

Cooper, O.R., Parrish, D.D., Stohl, A., Trainer, M., Nedelec, P., Thouret, V., et al., 2010. Increasing springtime ozone mixing ratios in the free troposphere over western North America. *Nature* 463 (7279), 344–348.

Fadeyi, M.O., 2015. Ozone in indoor environments: Research progress in the past 15 years. *Sustain. Cities. Soc.* 18, 78–94.

Gong, S.Y., Li, W.H., Xie, Z., Ma, X., Liu, H.D., Han, N., et al., 2017. Low temperature decomposition of ozone by facilely synthesized cuprous oxide catalyst. *New J. Chem.* 41 (12), 4828–4834.

Gong, S.Y., Chen, J.Y., Wu, X.F., Han, N., Chen, Y.F., 2018. In-situ synthesis of Cu_2O /reduced graphene oxide composite as effective catalyst for ozone decomposition. *Catal. Commun.* 106, 25–29.

Hao, Z.P., Cheng, D.Y., Guo, Y., Liang, Y.H., 2001. Supported gold catalysts used for ozone decomposition and simultaneous elimination of ozone and carbon monoxide at ambient temperature. *Appl. Catal. B* 33 (3), 217–222.

Hoffmann, B., Luttmann-Gibson, H., Cohen, A., Zanobetti, A., de Souza, C., Foley, C., et al., 2012. Opposing effects of particle pollution, ozone, and ambient temperature on arterial blood pressure. *Environ. Health Perspect.* 120 (2), 241–246.

Huang, Z.W., Gu, X., Cao, Q.Q., Hu, P.P., Hao, J.M., Li, J.H., et al., 2012. Catalytically active single-atom sites fabricated from silver particles. *Angew. Chem. Int. Ed.* 51 (17), 4198–4203.

Huang, Z.W., Gu, X., Wen, W., Hu, P.P., Makkee, M., Lin, H., et al., 2013. A "smart" hollandite denox catalyst: Self-protection against alkali poisoning. *Angew. Chem. Int. Ed.* 52 (2), 660–664.

Imamura, S., Sawada, H., Uemura, K., Ishida, S., 1988. Oxidation of carbon-monoxide catalyzed by manganese silver composite oxides. *J. Catal.* 109 (1), 198–205.

Imamura, S., Ikebata, M., Ito, T., Ogita, T., 1991. Decomposition of ozone on a silver catalyst. *Ind. Eng. Chem. Res.* 30 (1), 217–221.

Jia, J.B., Zhang, P.Y., Chen, L., 2016. Catalytic decomposition of gaseous ozone over manganese dioxides with different crystal structures. *Appl. Catal. B* 189, 210–218.

Kapteijn, F., Vanlangeveld, A.D., Moulijn, J.A., Andreini, A., Vuurman, M.A., Turek, A.M., et al., 1994. Alumina-supported manganese oxide catalysts. 1. Characterization - effect of precursor and loading. *J. Catal.* 150 (1), 94–104.

Kolathodi, M.S., Rao, S.N.H., Natarajan, T.S., Singh, G., 2016. Beaded manganese oxide (Mn_2O_3) nanofibers: Preparation and application for capacitive energy storage. *J. Mater. Chem. A* 4 (20), 7883–7891.

Li, L.Y., King, D.L., 2005. Synthesis and characterization of silver hollandite and its application in emission control. *Chem. Mater.* 17 (17), 4335–4343.

Li, J.M., Qu, Z.P., Qin, Y., Wang, H., 2016. Effect of MnO_2 morphology on the catalytic oxidation of toluene over Ag/ MnO_2 catalysts. *Appl. Surf. Sci.* 385, 234–240.

Li, Z.Y., Akhtar, M.S., Bui, P.T.M., Yang, O.B., 2017. Predominance of two dimensional (2D) Mn_2O_3 nanowalls thin film for high performance electrochemical supercapacitors. *Chem. Eng. J.* 330, 1240–1247.

Li, X.T., Ma, J.Z., Yang, L., He, G.Z., Zhang, C.B., Zhang, R.D., et al., 2018. Oxygen vacancies induced by transition metal doping in γ - MnO_2 for highly efficient ozone decomposition. *Environ. Sci. Technol.* 52, 12685–12696.

Lian, Z.H., Ma, J.Z., He, H., 2015. Decomposition of high-level ozone under high humidity over Mn-Fe catalyst: The influence of iron precursors. *Catal. Commun.* 59, 156–160.

- Liu, T.Z., Li, Q., Xin, Y., Zhang, Z.L., Tang, X.F., Zheng, L.R., et al., 2018. Quasi free K cations confined in hollandite-type tunnels for catalytic solid (catalyst)-solid (reactant) oxidation reactions. *Appl. Catal. B* 232, 108–116.
- Ma, J.Z., Wang, C.X., He, H., 2017. Transition metal doped cryptomelane-type manganese oxide catalysts for ozone decomposition. *Appl. Catal. B* 201, 503–510.
- Magzamen, S., Moore, B.F., Yost, M.G., Fenske, R.A., Karr, C.J., 2017. Ozone-related respiratory morbidity in a low-pollution region. *J. Occup. Environ. Med.* 59 (7), 624–630.
- Mehandjiev, D., Naidenov, A., 1992. Ozone decomposition on alpha-Fe₂O₃ catalyst. *Ozone Sci. Eng.* 14 (4), 277–282.
- Mehandjiev, D., Naydenov, A., Ivanov, G., 2001. Ozone decomposition, benzene and co oxidation over NiMnO₃-ilmenite and NiMn₂O₄-spinel catalysts. *Appl. Catal. A* 206 (1), 13–18.
- Naydenov, A., Konova, P., Nikolov, P., Klingstedt, F., Kumar, N., Kovacheva, D., et al., 2008. Decomposition of ozone on Ag/SiO₂ catalyst for abatement of waste gases emissions. *Catal. Today* 137 (2–4), 471–474.
- Qu, Z., Bu, Y., Qin, Y., Wang, Y., Fu, Q., 2013. The improved reactivity of manganese catalysts by Ag in catalytic oxidation of toluene. *Appl. Catal. B* 132–133, 353–362.
- Sun, Y.M., Hu, X.L., Zhang, W.X., Yuan, L.X., Huang, Y.H., 2011. Large-scale synthesis of Ag_{1.8}Mn₈O₁₆ nanorods and their electrochemical lithium-storage properties. *J. Nanopart. Res.* 13 (8), 3139–3148.
- Tang, W.X., Liu, H.D., Wu, X.F., Chen, Y.F., 2014. Higher oxidation state responsible for ozone decomposition at room temperature over manganese and cobalt oxides: Effect of calcination temperature. *Ozone Sci. Eng.* 36 (5), 502–512.
- Tuomi, T., Engstrom, B., Niemela, R., Svinhufvud, J., Reijula, K., 2000. Emission of ozone and organic volatiles from a selection of laser printers and photocopiers. *Appl. Occup. Environ. Hyg.* 15 (8), 629–634.
- Wang, C., Sun, L.A., Cao, Q.Q., Hu, B.Q., Huang, Z.W., Tang, X.F., 2011. Surface structure sensitivity of manganese oxides for low-temperature selective catalytic reduction of NO with NH₃. *Appl. Catal. B* 101 (3–4), 598–605.
- Wang, C.X., Ma, J.Z., Liu, F.D., He, H., Zhang, R.D., 2015. The effects of Mn²⁺ precursors on the structure and ozone decomposition activity of cryptomelane-type manganese oxide (OMS-2) catalysts. *J. Phys. Chem. C* 119 (40), 23119–23126.
- Xie, Y., Yu, Y., Gong, X., Guo, Y., Guo, Y., Wang, Y., et al., 2015. Effect of the crystal plane figure on the catalytic performance of MnO₂ for the total oxidation of propane. *CrystEngComm* 17 (15), 3005–3014.
- Xie, S.H., Liu, Y.X., Deng, J.G., Zhao, X.T., Yang, J., Zhang, K.F., et al., 2017. Effect of transition metal doping on the catalytic performance of Au-Pd/3DOM Mn₂O₃ for the oxidation of methane and o-xylene. *Appl. Catal. B* 206, 221–232.
- Yu, Q., Pan, H., Zhao, M., Liu, Z., Wang, J., Chen, Y., et al., 2009. Influence of calcination temperature on the performance of Pd-Mn/SiO₂-Al₂O₃ catalysts for ozone decomposition. *J. Hazard. Mater.* 172 (2–3), 631–634.
- Yu, K.P., Lee, G.W.M., Hsieh, C.P., Lin, C.C., 2011. Evaluation of ozone generation and indoor organic compounds removal by air cleaners based on chamber tests. *Atmos. Environ.* 45 (1), 35–42.
- Zhang, P.Y., Zhang, B., Shi, R., 2009. Catalytic decomposition of low level ozone with gold nanoparticles supported on activated carbon. *Front. Env. Sci. Eng.* 3 (3), 281–288.
- Zhou, L.N., Chen, Y.Q., Ren, C.J., Gong, M.C., 2013. Pd/MnO_x + Pd/gamma-Al₂O₃ monolith catalysts for ground-level ozone decomposition. *Chin. J. Inorg. Chem.* 29 (11), 2363–2369.
- Zhu, G.X., Zhu, J.G., Jiang, W.J., Zhang, Z.J., Wang, J., Zhu, Y.F., et al., 2017. Surface oxygen vacancy induced alpha-MnO₂ nanofiber for highly efficient ozone elimination. *Appl. Catal. B* 209, 729–737.